$NaGdF_4$ Nanoparticle-Based Molecular Probes for Magnetic Resonance Imaging of Intraperitoneal Tumor Xenografts *in Vivo*

Yi Hou,[†] Ruirui Qiao,[†] Fang Fang,[‡] Xuxia Wang,[‡] Chengyan Dong,[§] Kan Liu,[⊥] Chunyan Liu,[†] Zhaofei Liu,[§] Hao Lei,[‡,*] Fan Wang,[§] and Mingyuan Gao[†,*]

[†]Institute of Chemistry, Chinese Academy of Sciences, Bei Yi Jie 2, Zhong Guan Cun, Beijing 100190, China, [‡]Wuhan Center for Magnetic Resonance, State Key Laboratory of Magnetic Resonance and Atomic and Molecular Physics, Wuhan Institute of Physics & Mathematics, Chinese Academy of Sciences, Wuhan 430071, China, [§]Medical Isotopes Research Center, Peking University, Xueyuan Road 38, Beijing 100083, China, and [⊥]Cancer Hospital, CAMS & PUMC, Pan Jia Yuan Nan Li 17, Beijing 100021, China

ABSTRACT Differently sized $NaGdF_4$ nanocrystals with narrow particle size distributions were synthesized by a high temperature approach. Upon ligand exchange, the as-prepared hydrophobic $NaGdF_4$ nanocrystals were transferred into water by using asymmetric PEGs simultaneously bearing phosphate and maleimide groups. Further investigations demonstrated that the water-soluble $NaGdF_4$ nanocrystals, coated by PEG bearing two phosphate groups on the same side, exhibit not only excellent colloidal stability in water and PBS buffer, but also higher T1 relaxivity than Gd-DTPA (Magnevist). Through "click" reaction between the maleimide residue on particle surface and thiol group from the partly reduced anti-EGFR monoclonal antibody (mAb), $NaGdF_4$—PEG-mAb nanoprobes were constructed, and their biocompatibility and binding specificity were evaluated through *in vitro* experiments. A series of *in vivo* experiments were then carried out for detecting intraperitoneal tumor xenografts in nude mice by using magnetic resonance (MR) imaging technique. The results revealed that the $NaGdF_4$—PEG-mAb probes possessed satisfying tumor-specific targeting ability and strong MR contrast enhancement effects.

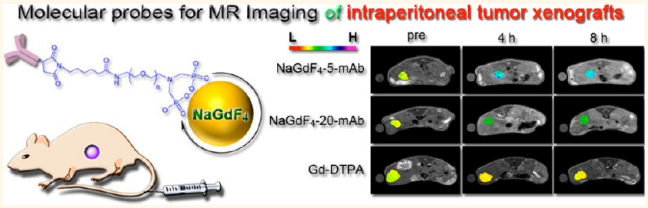

KEYWORDS: $NaGdF_4$ nanoparticles · ligand exchange · T1 contrast agent · MR molecular imaging probe · intraperitoneal tumor xenografts

Magnetic resonance imaging (MRI) has become one of the most important clinical tools nowadays for visualizing the internal structures of the body in detail.[1] Despite extremely high spatial and temporal resolutions, MRI still suffers from its poor ability in differentiating diseased and healthy tissues. Therefore, developing MRI contrast agents is highly demanded.[2,3]

To date, paramagnetic Gd-chelates dominate the MRI contrast agents used in clinical diagnosis,[4] meanwhile the nanoparticle-based MRI contrast agents have received increasing attention since FDA approved two magnetic iron oxide particle-based contrast agents in 1996.[5] Due to the enhanced vascular permeability, nanoparticles tend to be localized in tumor and therefore exhibit unique tumor-specific targeting ability in contrast to the paramagnetic metal chelates.[3,6] In addition, nanoparticle also offers a platform on which different types of functional moieties can be assembled for achieving multifunctional probes potentially useful for both diagnostic and therapeutic purposes.[7−9] So far, contrast agents based on superparamagnetic iron oxide particles have widely been investigated and evaluated in clinical trials of different stages.[5] In contrast, gadolinium-based paramagnetic nanoparticles as contrast agents are much less reported.[10−15]

In literature, the gadolinium-based paramagnetic nanocrystals are typically synthesized through the replacement reactions taking place between Gd^{3+} and anions such as F^-, PO_4^-, and OH^-, respectively, in water and polyol,[10−13] or the thermal decomposition reactions taking place in high boiling point organic solvents using different types of gadolinium-organic compounds as precursors.[14−18] The first approach is

* Address correspondence to gaomy@iccas.ac.cn, leihao@wipm.ac.cn.

Received for review September 3, 2012 and accepted November 30, 2012.

Published online November 30, 2012
10.1021/nn304837c

straightforward for producing hydrophilic nanocrystals such as GdF_3,[10,11] $GdPO_4$,[12] and Gd_2O_3,[13] etc., but the resultant nanocrystals are typically characterized by broad size distributions. In contrast, the second approach can give rise to nanocrystals with greatly improved size and shape uniformities. But it is only suitable for producing hydrophobic nanocrystals.

Aqueous solubility/dispersibility and colloidal stability are very important prerequisites for *in vivo* applications of any types of inorganic nanoparticles. Since the biodistribution, clearance rate, and elimination pathway of the intravenously injected nanoparticle are strongly associated with the particle size,[19−21] an effective size control over the monodispersed Gd^{3+}-containing nanocrystals and a suitable postpreparative approach for endowing the hydrophobic nanocrystals with aqueous colloidal stability are therefore equally important. Different methods for rendering the oleate-coated nanoparticles water-soluble have been reported recently.[14−18,22,23] Among them, overcoating the hydrophobic nanoparticles with SiO_2 has become the most popular one.[14] But the precise control over the thickness and shape of SiO_2 encapsulating layer remains challenging.[7,11,12] Other measures such as oxidizing the oleate ligand with ozone or potassium permanganate,[15,16] or replacing the oleate ligand with polyethylene glycol (PEG) or polyvinylpyrrolidone were also explored.[18,23] But $NaGdF_4$ nanoparticles with good colloid stability under physiological condition are rarely reported so far.

Herein, we report the preparation of nearly monodispersed $NaGdF_4$ nanocrystals, following a synthetic approach initially reported by Zhang.[14] The preparation was optimized so as to get differently sized $NaGdF_4$ nanocrystals stabilized by oleic acid. Upon ligand exchange, water-soluble $NaGdF_4$ particles bearing surface reactive maleimide (mal) groups were obtained. Through efficient "click" reaction,[24] tumor-specific MRI probes were constructed, evaluated, and subsequently used in detecting intraperitoneal tumor xenografts in nude mice.

RESULTS AND DISCUSSION

Synthesis and Characterization of $NaGdF_4$ Nanoparticles. In brief, $NaGdF_4$ nanocrystals were prepared by a high temperature approach through the replacement reaction between $GdCl_3$ and NH_4F taking place in the presence of excess NaOH. Oleic acid (OA) was chosen as a particle surface capping agent. It also served as solvent together with 1-octadecene. The particle size and size distribution shown in Figure S1 in Supporting Information (SI) reveal that the $NaGdF_4$ particle growth undergoes a size broadening process at 300 °C, followed by a size focusing process, suggesting that the Ostwald ripening process plays an important role determining both particle size and size distribution in the current reaction system.[14] Therefore, the reaction temperature and time were optimized so as to vary the size of $NaGdF_4$ nanoparticles and meanwhile narrow their size distribution.

The transmission electron microscopy (TEM) images shown in Figure 1 demonstrate that the size of monodispersed particles obtained can effectively be tuned by different combinations of the reaction time and temperature, for example, 45 min at 270 °C to achieve 5.4 ± 0.8 nm $NaGdF_4$ ($NaGdF_4$-5), 60 min at 300 °C to get 15.1 ± 0.8 nm $NaGdF_4$ ($NaGdF_4$-15), and 60 min at 320 °C to obtain 19.8 ± 1.0 nm $NaGdF_4$ ($NaGdF_4$-20), respectively, which marks the difference of the current synthetic route from previous ones by its strong particle size tunability.[18] Further powder X-ray diffraction (XRD) studies reveal that $NaGdF_4$-5 is in the cubic-phase, while $NaGdF_4$-15 and $NaGdF_4$-20 are in the hexagonal-phase.

Preparation and Characterization of Water-Soluble $NaGdF_4$ Nanoparticles. To render the $NaGdF_4$ nanocrystals stabilized by oleic acid water-soluble, asymmetric polyethylene glycols (PEGs) carrying a maleimide group at one end and one or two phosphate groups at the other end, denoted as mal-PEG-mp and mal-PEG-dp, respectively, were used to replace the oleate ligand of the as-prepared $NaGdF_4$ nanocrystals based on the fact that the phosphate group has a higher binding affinity to Gd^{3+} than the carboxyl group from oleic acid. The detail chemical structures of mal-PEG-mp and mal-PEG-dp are shown in Scheme 1. Dynamic light scattering (DLS) analysis was carried out to characterize the aqueous dispersion of the resultant nanoparticles. As shown in Figure 2a, $NaGdF_4$-20 particles stabilized by mal-PEG-mp exhibit a relatively narrow particle size distribution in water with a single scattering peak locating at 51 nm. The DLS result on the one hand suggests that PEG-phosphate can effectively replace oleate ligand, on the other hand indicates that the ligand exchange process took place in a controlled way that no unwanted agglomeration of the particles occurred.

Satisfying colloidal stability is a very important prerequisite for exploring the biomedical applications of nanomaterials since this stability strongly governs the blood circulation behavior of the nanoparticles administrated *via* intravenous injection and the consequent particle biodistribution as well. Therefore, the colloidal stability of (mal-PEG-mp)-coated $NaGdF_4$ particles in water and phosphate buffered saline (PBS) that is commonly used to mimic the human biological conditions was evaluated by DLS method. As shown in Figure 2b, (mal-PEG-mp)-coated $NaGdF_4$-20 particles present excellent colloidal stability in pure water. However, they quickly flocculate in 1× PBS as illustrated by the drastic increase in the hydrodynamic size of the particle aggregates. The quick flocculation is mainly caused by the replacement of mal-PEG-mp ligand by phosphate ion in PBS as the latter is very

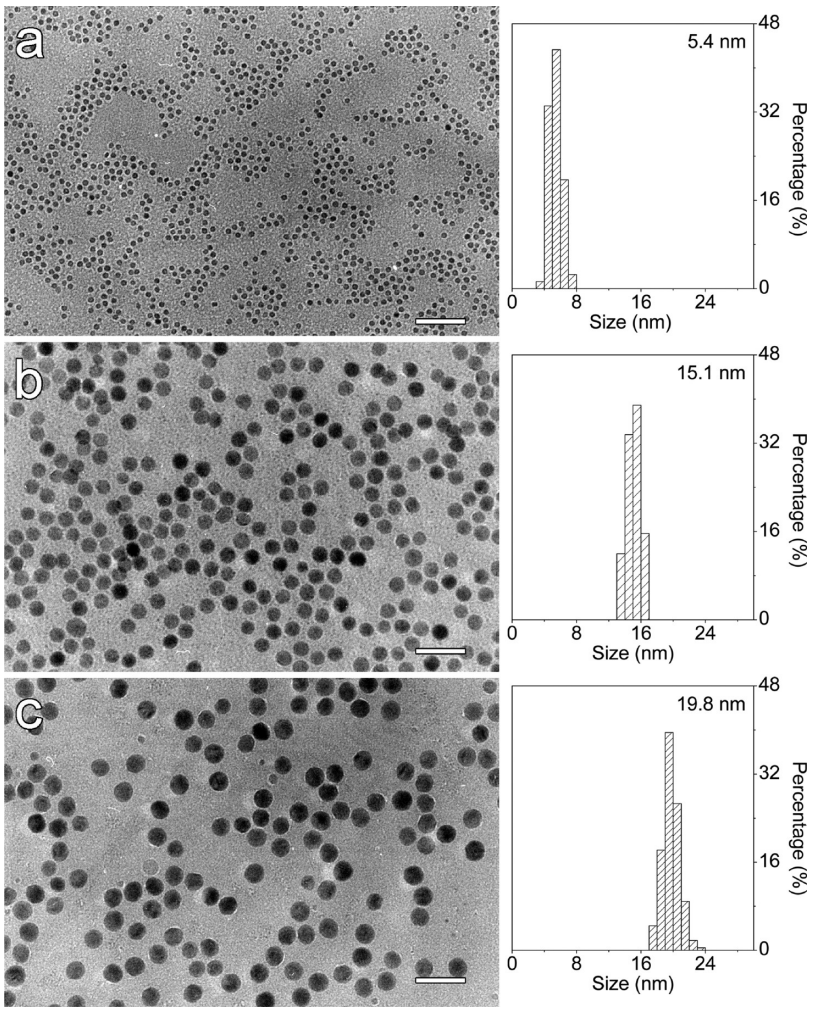

Figure 1. TEM images and histograms of the as-prepared $NaGdF_4$ nanoparticles: $NaGdF_4$-5 (a), $NaGdF_4$-15 (b), and $NaGdF_4$-20 (c). The scale bars correspond to 50 nm.

excessive in the system.[23] To solve this problem, mal-PEG-dp was adopted instead of mal-PEG-mp to exchange the oleate ligand of the $NaGdF_4$ nanoparticles so as to enhance the colloidal stability of the resultant nanoparticles in phosphate buffer solution. The temporal evolutions of the hydrodynamic size of (mal-PEG-dp)-coated $NaGdF_4$-20 particles in both water and PBS, as shown in Figure 2c, strongly support that mal-PEG-dp ligand can more effectively prevent $NaGdF_4$ nanocrystals from forming aggregates under physiological conditions. The greatly improved colloidal stability can be interpreted by the multidentate Gd^{3+} binding ability of the diphosphate group. Further experimental observation demonstrated that the (mal-PEG-dp)-coated $NaGdF_4$ nanocrystals remained colloidally stable in PBS since they were prepared more than 1 year ago.

Relaxivity Measurement *in Vitro* and Cytotoxicity of PEG-Coated $NaGdF_4$ Nanoparticles. The performance of the (mal-PEG-dp)-coated $NaGdF_4$ nanoparticles as MRI contrast agents was evaluated on a clinic 3T MRI scanner. The experimentally determined longitudinal relaxivity R1 of water protons was plotted against the molar concentration of Gd^{3+}. The molar relaxivity r1 extracted from the linear regression fits of the experimental data, as shown in Figure 3a, is of 6.20 mM^{-1} s^{-1} for $NaGdF_4$-5, 5.7 mM^{-1} s^{-1} for $NaGdF_4$-15, 8.78 mM^{-1} s^{-1} for $NaGdF_4$-20, and 3.15 mM^{-1} s^{-1} for Gd-DTPA (DTPA = diethylenetriaminepentaacetate). In comparison with Gd-DTPA, the first paramagnetic contrast agent marketed as Magnevist for clinical use, the $NaGdF_4$ nanoparticles present greatly enhanced r1 that shows a nonmonotonic behavior against the particle size. This can qualitatively be interpreted by the following particle size-related effects. On the one hand, r1 relaxivity should decrease with the $NaGdF_4$ particle size since the amount of surface Gd^{3+}, the main driving force for shortening the longitudinal relaxation of water protons nearby, decreases against the particle size at a given concentration of Gd^{3+}.[18] On the other hand, this effect may be counteracted by the decreased tumbling time for larger particles. In fact, according to the impact of a contrast agent on the relaxation of water protons, the surrounding water can be divided into three distinct regions: inner sphere, secondary sphere, and outer

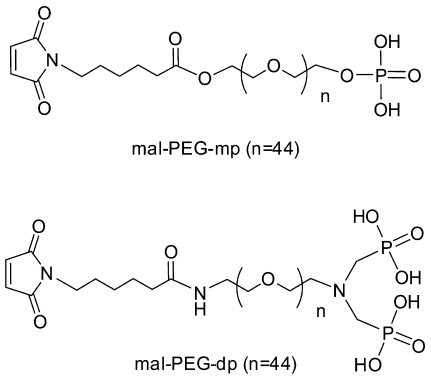

Scheme 1. Molecular structures of mal-PEG-mp and mal-PEG-dp ligands.

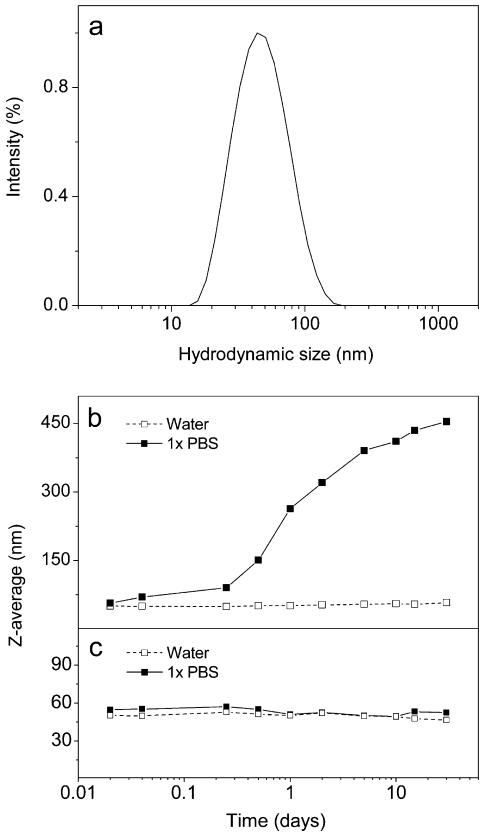

Figure 2. Hydrodynamic size profile of the (mal-PEG-dp)-coated $NaGdF_4$-20 nanoparticles (a), and temporal evolutions of the hydrodynamic sizes of the (mal-PEG-mp)-coated (b) and the (mal-PEG-dp)-coated $NaGdF_4$-20 nanoparticles (c) in water and 1 × PBS, respectively.

sphere.[24] The relaxation of magnetization of water protons in the secondary and outer spheres are mainly contributed by the water molecules bonded to the particle surface ligands and their exchange with bulk water.[25] Therefore, it can be deduced that the water protons in the inner sphere contribute to the particle size-dependent r1 relaxivity since the surface ligands for these three particle samples are the same for the present study. The longitudinal relaxivity of water protons in the inner sphere is strongly dependent on the tumbling time of the contrast agent, that is, the

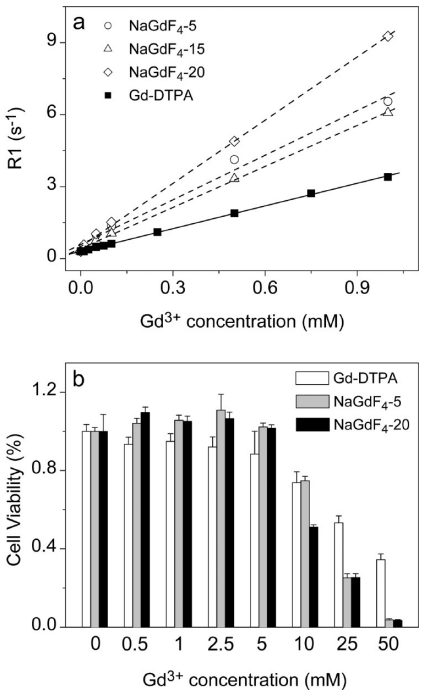

Figure 3. (a) R1 relaxivity of aqueous solutions containing differently sized nanoparticles or Gd-DTPA with different concentrations of Gd^{3+}; (b) cell viability of GC7901 cells incubated with (mal-PEG-dp)-coated $NaGdF_4$ particles or Gd-DTPA with different Gd^{3+} concentrations.

$NaGdF_4$ particle in the current case.[18] In principle, slowing the tumbling of Gd^{3+} ions is in favor of higher r1 relaxivity, while the tumbling time decreases as the nanoparticle size increases. This may explain why $NaGdF_4$-20 presents a higher r1 than $NaGdF_4$-15. Although the aforementioned two particle size-dependent effects on r1 can help to qualitatively understand the particle size dependency of r1, more systematic investigations are still needed for further quantitatively interpreting the particle size-dependent r1. Nonetheless, the current results give strong enough reason to further study $NaGdF_4$-5 and $NaGdF_4$-20 as they both present enhanced relaxivity in comparison with $NaGdF_4$-15 apart from a bigger mutual difference in size.

Before further *in vitro* and *in vivo* experiments, the cytotoxicity of the (mal-PEG-dp)-coated $NaGdF_4$-5 and $NaGdF_4$-20 was first evaluated through MTT (3-(4,5-dimethylthiazol-2-yl)-2,5-diphenyltetrazolium bromide) cell proliferation assays on GC7901 cells. The results are shown in Figure 3b. In comparison with Gd-DTPA, both $NaGdF_4$-5 and $NaGdF_4$-20 give rise to enhanced cell viability when the concentration of Gd^{3+} is below 5 mM. However, the $NaGdF_4$ nanoparticles start to decrease the cell viability when the concentration of Gd^{3+} is higher than 10 mM, more dramatically than Gd-DTPA. Theoretical fittings reveal that the IC_{50} (50% inhibitory concentration) values of $NaGdF_4$-5 and $NaGdF_4$-20 are of 16.5 and 13.8 mM, respectively. Since the highest clinical dose for Gd-DTPA is around 0.3 mmol·kg^{-1},[4] roughly corresponding to 0.3 mM, it is reasonable to

believe that the current $NaGdF_4$-5 and $NaGdF_4$-20 are on the safe side for being used as contrast agent in MR imaging, at least for animal studies.

Conjugation of anti-EGFR mAb to $NaGdF_4$ Nanoparticles. Two tumor-specific MR molecular probes were prepared by covalently conjugating anti-EGFR monoclonal antibody (mAb) to the $NaGdF_4$-5 and $NaGdF_4$-20 through the "click" reaction between the maleimide residue on particle surface and thiol group from the partly reduced anti-EGFR mAb.[26] The effectiveness of the coupling reaction was first evaluated by DLS. The results shown in Figure S2 in the SI reveal that the hydrodynamic size of $NaGdF_4$-20 increases from 51 to 57 nm after the coupling reaction and the size distribution profile of the conjugates remains nearly unchanged in comparison with that of the mother particles, which strongly supports that the mAb molecules are effectively coupled to the nanoparticles. Further spectroscopy studies demonstrated that the resultant conjugates were formed through the maleimide−thiol "click" reaction rather than the nonspecific adsorption of mAb on the particles (more details are provided in Figure S3 in SI).

Maintaining the bioactivity of anti-EGFR mAb is of the utmost importance for the following application of the resultant $NaGdF_4$−PEG-mAb conjugates. The bioactivity of the $NaGdF_4$−PEG-mAb conjugates was quantitatively evaluated through cell binding assays in which human epithelial carcinoma cell line A431 and human breast carcinoma cell line MDA-MB-435 were used as positive and negative controls,[27,28] respectively. The difference in the binding affinity of the $NaGdF_4$−PEG-mAb probe to A431 and its control MDA-MB-435 can qualitatively be visualized from the fluorescence micrographs shown in the upper panel of Figure 4. The quantitative analysis through ICP−AES measurements revealed that the amount of $NaGdF_4$-20 in A431 cells was 10-fold of that in MDA-MB-435 after they were treated with the nanoprobes, suggesting that the $NaGdF_4$−PEG-mAb conjugates possess excellent binding specificity to tumor cells overexpressed with EGFR on the surface. In addition, murine immunoglobulin G (mIgG) was chosen to construct a control conjugate, that is, $NaGdF_4$−PEG-mIgG, for cell binding assays. The results shown in the lower panel of Figure 4 strongly support that the binding specificity of the $NaGdF_4$−PEG-mAb conjugate is endowed by the specific interaction between EGFR and anti-EGFR antibody, while the nonspecific uptake of the irrelevant $NaGdF_4$−PEG-mIgG probe is rather weak.

***In Vivo* MR Imaging of Intraperitoneal Tumor Xenografts.** In previous investigations, the subcutaneously xenografted tumors were the most commonly used tumor model for molecular imaging studies using nanoparticle-based molecular probes.[5,8] In the current study, the intraperitoneally xenografted tumor model was used instead for better reflecting the nature of colorectal

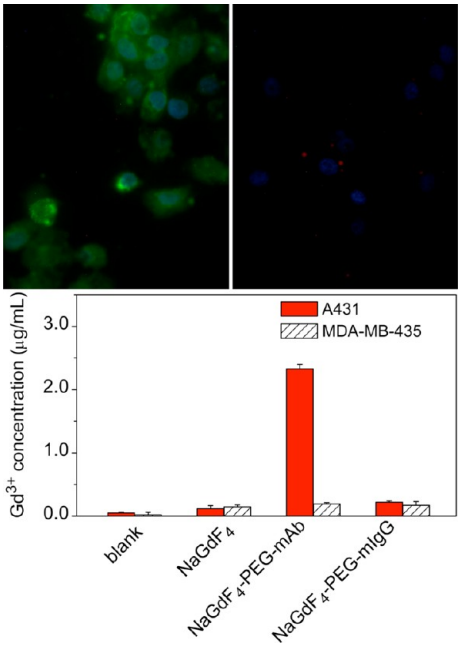

Figure 4. (Upper panel) Fluorescence images of A431 cells (left) and MDA-MB-435 cells (right) stained by $NaGdF_4$−PEG-mAb probes and Hochest 33342 for cell membrane and nucleus, respectively; (lower panel) Gadolinium concentrations in A431 and MDA-MB-435 cell samples determined after they were treated with $NaGdF_4$, $NaGdF_4$−PEG-mAb, and $NaGdF_4$−PEG-mIgG, respectively, while the gadolinium concentrations of untreated A431 cells and MDA-MB-435 samples are shown as "blank".

cancer as the latter can also be taken as a metastatic model.[29] On the basis of the aforementioned systematic characterizations as well as successful *in vitro* experiments, $NaGdF_4$−PEG-mAb probes were used in the following *in vivo* experiments for detecting colorectal tumors in BALB/c nude mice, and the corresponding mother particles and Gd-DTPA were used as negative controls. Since the $NaGdF_4$−PEG-mIgG probe did not present enhanced interactions with A431 cells *in vitro* in comparison with the corresponding mother particle, it was not further adopted as a control for further *in vivo* imaging experiments. T1-weighted MR images acquired before and at different time points postinjection are provided in the upper panel of Figure 5. It is quite evident that the $NaGdF_4$−PEG-mAb probes present clear tumor targeting ability *in vivo*. In contrast, Gd-DTPA hardly enhances the contrast of the tumor region under the same experimental conditions, as shown in Figure S4 in SI. The tumor-targeting behaviors of the $NaGdF_4$−PEG-mAb probes can clearly be seen from the quantitative analysis on the temporal evolutions of T1 values in the tumor regions, as shown in the lower frames in Figure 5. In general, the T1 values of the tumor site start to decrease shortly after the injection of $NaGdF_4$−PEG-mAb probes, reaching a minimum at ~4 h postinjection by $\Delta T1$ of ~50% for $NaGdF_4$-5-mAb and 30% for $NaGdF_4$-20-mAb. Although the mother particles also present similar temporal

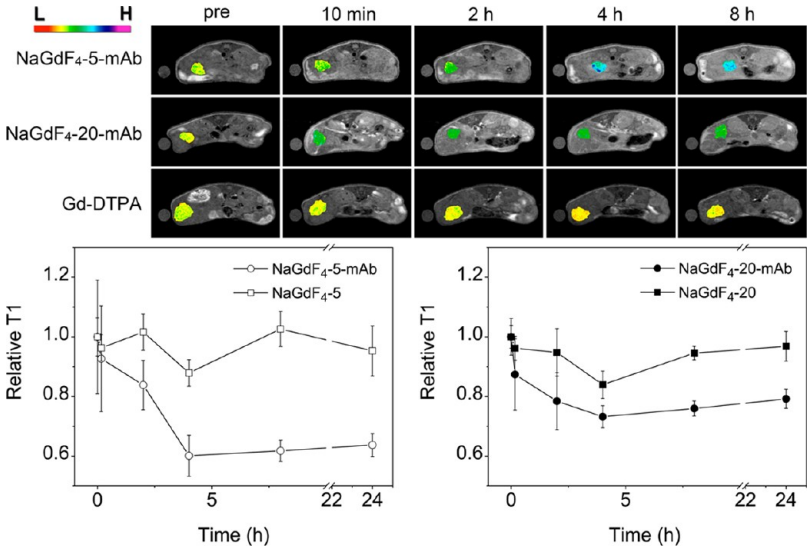

Figure 5. (Upper frame) T1-weighted MR images of tumor-bearing mice acquired before and at different time points after the intravenous injections of Gd-DTPA (row 3) or $NaGdF_4$—PEG-mAb probes formed by using $NaGdF_4$-5 (row 1) and $NaGdF_4$-20 (row 2), respectively. (Lower frame) T1 values extracted before and after the injections of $NaGdF_4$—PEG-mAb probes or the corresponding mother particles from the tumor sites color-coded to better show the contrast enhancement effects of the particle probes.

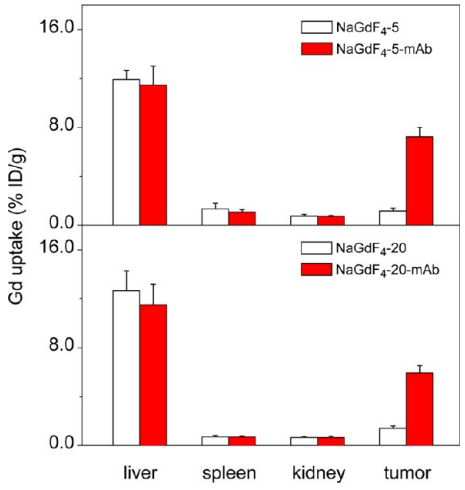

Figure 6. Biodistributions of $NaGdF_4$-5, $NaGdF_4$-5-mAb, $NaGdF_4$-20, and $NaGdF_4$-20-mAb in tumor and main organs of mice, determined 24 h after they were intravenously injected, respectively.

behaviors, quite probably caused by the enhanced permeability and retention effect associated with tumor, the resulting Δ T1 is much lower (<15%). It should be mentioned that the variation of the relative tumor position in the same mouse is mainly caused by the displacement of the internal organs and tumor induced by repeatedly fixing the mouse on a respiration sensor for monitoring the living status of the mice under anesthesia during the MRI experiments.

To provide further support to the tumor-specific targeting ability as well as information on the biodistribution of the $NaGdF_4$—PEG-mAb probes, both tumors and important organs such as liver, spleen, and kidney were harvested after the *in vivo* experiments. Then Gd contents in the tumor tissue and different organs were analyzed by ICP—AES. The results on tumor uptakes of the $NaGdF_4$—PEG-mAb probes and the mother particles, as shown in Figure 6, are generally well in consistency with the imaging results shown in Figure 5. In comparison with similarly structured tumor probes based on Fe_3O_4 particles,[8] the current $NaGdF_4$—PEG-mAb probes present greatly enhanced tumor uptake efficacies, by at least a factor of 2.4, if the corresponding liver uptake is used as internal reference representing the mononuclear phagocyte system. Nevertheless, similar to most particulate probes, the liver uptakes of the probes and the control particles remain in spite of reduced levels. It should also be pointed out that the data shown in Figure 6, as follow-up results of the *in vivo* experiments, are far from complete for describing the pharmacokinetics of the new probes reported herein. In addition, nothing is known about the clearance rate and elimination pathways of current probes at present. But the current investigations have demonstrated that the $NaGdF_4$ nanocrystals as T1 contrast agents are potentially useful for constructing MRI probes for *in vivo* tumor imaging, as an alternative choice of T2 contrast agents formed by iron oxide nanoparticles, at least for animal studies.

CONCLUSIONS

In summary, the asymmetric PEGs simultaneously bearing phosphate and maleimide groups were designed and used to exchange the oleate ligand of $NaGdF_4$ nanocrystals, on the one hand for rendering them water-soluble and on the other hand for further covalently conjugating tumor-specific ligand to the nanoparticle to form molecular probe for MR imaging

of tumors. Systematic studies demonstrated that PEG-phosphate can effectively replace the oleate ligand, but the PEG bearing single phosphate group cannot firmly anchor on the particle surface in PBS. In contrast, the PEG ligand carrying two phosphate groups on the same side presents greatly improved binding affinity to the $NaGdF_4$ nanocrystals. Consequently, the $NaGdF_4$ nanocrystals exhibit long-term colloidal stability in both water and PBS buffer. In addition, the water-soluble $NaGdF_4$ nanoparticles also present superior contrast agent properties to Gd-DTPA. *Via* maleimide group, EGFR-targeting probes are prepared by covalently conjugating anti-EGFR mAb to $NaGdF_4$ nanoparticles through the high efficient "click" reaction. Careful cell binding assays demonstrate that the $NaGdF_4$—PEG-mAb probes possess excellent binding specificity to EGFR expressed on tumor cells. Further *in vivo* experiments prove that the $NaGdF_4$—PEG-mAb probes present satisfying tumor-specific targeting ability and strong MR contrast enhancement effects in the intraperitoneal xenograft tumor model that is in many aspects superior to the subcutaneous xenograft tumor model widely used in literature for mimicking the intraperitoneal metastasis of colorectal cancers. We therefore believe that the current investigations have paved a reliable way for exploring the *in vivo* applications of lanthanide-based nanoparticles, especially in molecular imaging of tumors.

EXPERIMENTAL SECTION

Chemicals. The following materials were purchased from Sigma-Aldrich: $GdCl_3 \cdot 6H_2O$, oleic acid (OA), 1-octadecene (ODE), ammonium fluoride (NH_4F), tris(2-carboxyethyl) phosphine hydrochloride (TCEP), and methyl thiazolyl tetrazolium (MTT). Analytical grade chemicals such as ethanol, cyclohexane, and tetrahydrofuran (THF) were purchased from Sinopharm Chemical Reagent Beijing, Co., Ltd. PEGs ($M_w \approx 2000$) with one or two phosphate groups at one end of the chain and a maleimide group at the other end were customized products provided by Beijing Oneder Hightech Co. Ltd. Human gastric cancer cell line GC7901, human epithelial carcinoma cell line A431, human breast carcinoma cell line MDA-MB-435, and human colorectal cancer cell line LS180 were obtained from the Oncology School of Peking University. Monoclonal anti-EGFR antibody (Erbitux) was purchased from Boehringer Ingelheim Pharma GmbH & Co KG. Murine immunoglobulin G (mIgG) was purchased from Sigma (I5381).

Preparation of $NaGdF_4$ Nanoparticles. In a typical preparation, $GdCl_3 \cdot 6H_2O$ (0.371 g, 1 mmol) was dissolved in a mixture of OA (14 mL) and ODE (16 mL).The solution was heated to 150 °C under nitrogen protection to form a homogeneous solution, into which 10 mL of methanol solution containing NaOH (0.100 g, 2.5 mmol) and NH_4F (0.148 g, 4 mmol) was then slowly added after it was cooled down to room temperature. After that, the reaction mixture was kept under stirring at 50 °C for 30 min, at 100 °C under vacuum for 10 min to remove methanol, and then heated to 300 °C under atmospheric pressure by electromantle, and maintained at 300 °C for 1 h under nitrogen protection. The preparation was terminated by cooling the reaction mixture down to room temperature. The resultant nanoparticles, that is, $NaGdF_4$-15, were precipitated by ethanol, collected by centrifugation, washed with ethanol several times, and finally redispersed in THF or cyclohexane for further experiments.

Ligand Exchange. As a typical example, 100 mg of PEG-phosphate ligand was mixed with *ca.* 10 mg OA-coated $NaGdF_4$ nanoparticles in 10 mL of THF. Then, the reaction mixture was kept overnight at room temperature under stirring. The PEG-coated particles were precipitated by cyclohexane, washed with cyclohexane for three times, and finally dried under vacuum at room temperature. The PEG-coated $NaGdF_4$ particles obtained in this way, independent of the particle size, were found to be readily dissolved in aqueous media.

Relaxivity Measurements. The relaxivity measurements were carried out on a 3 T clinical MRI instrument (GE signa 3.0T HD, Milwaukee, WI). A series of aqueous solutions of (mal-PEG-dp)-coated $NaGdF_4$ particles in 1.5 mL Eppendorf tubes were prepared. The parameters for T1 measurements were set as follows: echo time (TE) = 15.3 ms; repetition time (TR) = 500, 1000, 1500, 2000 ms; number of excitations (NEX) = 8.

Cytotoxicity of PEG-Coated $NaGdF_4$ Nanoparticles. MTT assays on GC7901 cells were carried out as follows. Cells were seeded into a 96-well cell culture plate by 2×10^3 cells/well under 100% humidity, and then cultured at 37 °C in an atmosphere containing 5% CO_2 for 24 h. The (mal-PEG-dp)-coated $NaGdF_4$ nanoparticles were added to the wells at designed concentrations, and incubated with the cells for 24 h at 37 °C under 5% CO_2. Subsequently, the supernatant containing the (mal-PEG-dp)-coated $NaGdF_4$ nanoparticles was decanted, and the cells were incubated for another 48 h at 37 °C under 5% CO_2. Thereafter, MTT (10 μL, 5 mg/mL) was added to each well and incubated for 4 h at 37 °C under 5% CO_2. After addition of 100 μL of DMSO per well, the assay plate was shaken at 37 °C for 10 min. The optical density of each well at 570 nm was recorded on a microplate reader (Thermo, Varioskan Flash), while the optical density at 690 nm was used as reference.

Preparation of $NaGdF_4$—PEG-mAb Conjugates. Typically, anti-EGFR mAb (1 mg/mL in 10× PBS) was subjected to mild reduction by TCEP to convert the disulfide groups in the Fc fragments to thiols. The reduction and subsequent purification was performed in 1.5 mL of 30 K MWCO centrifugal devices (Millipore YM-30). The following conjugation reaction was performed by mixing (mal-PEG-dp)-coated $NaGdF_4$ nanoparticles with the partially reduced anti-EGFR mAb in Tris-buffered saline (TBS, pH 7.4). In principle, the yield of the "click" reaction between maleimide and thiol groups is close to 100%. In the current imaging probe preparation, the concentration of antibody was much smaller than that of the maleimide residue from the particle surface. Nevertheless, the $NaGdF_4$—PEG-mAb conjugates were purified by centrifugation for 3 times at 16000*g* to remove the unreacted antibody, and then stored at 4 °C. FITC-labeled anti-EGFR mAb was also used to prepare fluorescent particle probes following the above procedures.

Binding Specificity of $NaGdF_4$—PEG-mAb Conjugates. Fluorescence microscopy was used for qualitative evaluation of the binding specificity of the $NaGdF_4$—PEG-mAb probes to A431 and MDA-MB-435 cells. In detail, approximately 1×10^5 A431 and MDA-MB-435 cells were seeded in the wells of two 8-well chamber slides, respectively, and incubated overnight at 37 °C under 5% CO_2 to allow a firm adherence. After being rinsed with PBS buffer, the cells were incubated with $NaGdF_4$—PEG-mAb conjugates labeled by FITC at 37 °C under 5% CO_2 for 1 h. After that, the cells were rinsed three times with PBS buffer. The fluorescence micrographs were captured using a fluorescence microscope (Olympus X71). The cell-associated Gd^{3+} was determined by using inductively coupled plasma-atomic emission spectrometer (ICP-AES) after the cells were eroded by 3 M HNO_3.

Animal Tumor Model. The tumor model used was established upon intraperitoneal injection of $\sim 5 \times 10^6$ LS180 cells into 4—6 weeks old male BALB/c nude mice. The tumor imaging studies were carried out when the tumor volume reached 180—240 mm^3 (~10 days after inoculation). All the experiments were performed according to a protocol approved by the Peking University Institutional Animal Care and Use Committee.

***In Vivo* MR Imaging of Intraperitoneal Tumor Xenografts.** Nude mice bearing LS180 tumors in the enterocoelia regions were anesthetized, and then *via* tail vein the $NaGdF_4$—PEG-mAb probe, the mother particle, or Gd-DPTA was injected by 0.1 mmol Gd^{3+} per kg body weight. MR imaging was conducted on a 4.7 T/30 cm Bruker Biospec animal MRI instrument using a saturation-recovery spin—echo imaging sequence. The imaging parameters were set as follows: field of view (FOV) = 3.5 × 4.5 cm^2; matrix size = 128 × 128; slice thickness = 1 mm; echo time (TE) = 11 ms; repetition time (TR) = 90, 150, 300, 500, 800, 1200, 2000, and 3000 ms; number of excitations (NEX) = 4. T1 maps were calculated by pixel-wise fitting of the TR-dependent signal intensity changes to a single exponential function. The mice were anesthetized by 1% isoflurane delivered *via* a nose cone during the imaging sessions. After acquiring the images at 10 min and 2 h postinjection, the animals were taken out from the magnet and allowed to recover from the anesthesia. Then, the animals were reanesthetized for acquiring the images at 4 and 8 h postinjection. The above procedures were repeated until acquisition of postinjection images was ended at 24 h. The uptakes of the $NaGdF_4$ probes and the mother particles by tumor and organs were determined by using ICP—AES after they were eroded by HNO_3 and H_2O_2.

Characterizations. TEM images of the nanocrystals were taken on a JEM-100CXII electron microscope at an acceleration voltage of 100 kV. The particle size was determined by counting at least 300 nanocrystals per sample. Powder XRD patterns of the particle samples were recorded on a Regaku D/Max-2500 diffractometer under Cu $K\alpha_1$ radiation (λ = 1.54056 Å). DLS measurements were carried out at 298.0 K with Nano ZS (Malvern) equipped with a solid state He—Ne laser (λ = 632.8 nm) for determining the hydrodynamic size of the PEG-coated $NaGdF_4$ and monitoring the following bioconjugation reaction. The concentration of Gd^{3+} was determined by using an inductively coupled plasma atomic emission spectrometer (ICP-2000) produced by Jiangsu Skyray Instrument Co., Ltd.

Conflict of Interest: The authors declare no competing financial interest.

Acknowledgment. The authors thank the National Basic Research Program of China (2011CB935800), NSFC (81090271, 21003135, 20820102035, 21021003), and CAS (KJCX2-YW-M15) for financial support. M.G. is grateful to Prof. Guojun Zhang from the Cancer hospital, Shantou University Medical College for helpful discussion.

Supporting Information Available: Additional figures as described in the text. This material is available free of charge *via* the Internet at http://pubs.acs.org..

REFERENCES AND NOTES

1. Bottrill, M.; Nicholas, L. K.; Long, N. Lanthanides in Magnetic Resonance Imaging. *J. Chem. Soc. Rev.* **2006**, *35*, 557–571.
2. Caravan, P.; Ellison, J. J.; McMurry, T. J.; Lauffer, R. B. Gadolinium(III) Chelates as MRI Contrast Agents: Structure, Dynamics, and Applications. *Chem. Rev.* **1999**, *99*, 2293–2352.
3. Lee, J. H.; Huh, Y. M.; Jun, Y. W.; Seo, J. W.; Jang, J. T.; Song, H. T.; Kim, S.; Cho, E. J.; Yoon, H. G.; Suh, J. S.; *et al.* Artificially Engineered Magnetic Nanoparticles for Ultra-Sensitive Molecular Imaging. *Nat. Med.* **2007**, *13*, 95–99.
4. Caravan, P. Strategies for Increasing the Sensitivity of Gadolinium-Based MRI Contrast Agent. *Chem. Soc. Rev.* **2006**, *35*, 512–523.
5. Qiao, R. R.; Yang, C. H.; Gao, M. Y. Superparamagnetic Iron Oxide Nanoparticles: From Preparations to *in Vivo* MRI Applications. *J. Mater. Chem.* **2009**, *19*, 6274–6293.
6. Hu, F. Q.; Wei, L.; Zhou, Z.; Ran, Y. L.; Li, Z.; Gao, M. Y. Preparation of Biocompatible Magnetite Nanocrystals for *in Vivo* Magnetic Resonance Detection of Cancer. *Adv. Mater.* **2006**, *18*, 2553–2556.
7. Huh, Y. M.; Jun, Y. W.; Song, H. T.; Kim, S.; Choi, J. S.; Lee, J. H.; Yoon, S.; Kim, K. S.; Shin, J. S.; Suh, J. S.; *et al. In Vivo* Magnetic Resonance Detection of Cancer by Using Multifunctional Magnetic Nanocrystals. *J. Am. Chem. Soc.* **2005**, *127*, 12387–12391.
8. Liu, S. J.; Jia, B.; Qiao, R. R.; Yang, Z.; Yu, Z. L.; Liu, Z. F.; Liu, K.; Shi, J. Y.; Ouyang, H.; Wang, F.; *et al.* A Novel Type of Dual-Modality Molecular Probe for MR and Nuclear Imaging of Tumor: Preparation, Characterization and *in Vivo* Application. *Mol. Pharm.* **2009**, *6*, 1074–1082.
9. Chen, K.; Xie, J.; Xu, H. Y.; Behera, D.; Michalski, M. H.; Biswal, S.; Wang, A.; Chen, X. Y. Triblock Copolymer Coated Iron Oxide Nanoparticle Conjugate for Tumor Integrin Targeting. *Biomaterials* **2009**, *30*, 6912–6919.
10. Vanics, F.; Diamente, P. R.; van Veggel, F. C. J. M.; Stanisz, G. J.; Prosser, R. S. Water-Soluble GdF_3 and GdF_3/LaF_3 Nanoparticles Physical Characterization and NMR Relaxation Properties. *Chem. Mater.* **2006**, *18*, 2499–2505.
11. Sun, C.; Veiseh, O.; Gunn, J.; Fang, C.; Hansen, S.; Lee, D.; Sze, R.; Ellenbogen, R. G.; Olson, J.; Zhang, M. *In Vivo* Detection of Gliomas by Chlorotoxin-Conjugated Superparamagnetic Nanoprobes. *Small* **2008**, *4*, 372–379.
12. Hifumi, H.; Yamaoka, S.; Tanimoto, A.; Citterio, D.; Suzuki, K. Gadolinium-Based Hybrid Nanoparticles as a Positive MR Contrast Agent. *J. Am. Chem. Soc.* **2006**, *128*, 15090–15091.
13. Bridot, J. L.; Faure, A. C.; Laurent, S.; Riviere, C.; Billotey, C.; Hiba, B.; Janier, M.; Josserand, V.; Coll, J. L.; Vander Elst, L.; *et al.* Hybrid Gadolinium Oxide Nanoparticles: Multimodal Contrast Agents for *in Vivo* Imaging. *J. Am. Chem. Soc.* **2007**, *129*, 5076–5084.
14. Li, Z. Q.; Zhang, Y.; Jiang, S. Multicolor Core/Shell-Structured Upconversion Fluorescent Nanoparticles. *Adv. Mater.* **2008**, *20*, 4765–4769.
15. Zhou, H. P.; Xu, C. H.; Sun, W.; Yan, C. H. Clean and Flexible Modification Strategy for Carboxyl/Aldehyde-Functionalized Upconversion Nanoparticles and Their Optical Applications. *Adv. Funct. Mater.* **2009**, *19*, 3892–3900.
16. Zhou, J.; Sun, Y.; Du, X. X.; Xiong, L. Q.; Hu, F.; Li, F. Y. Dual-Modality *in Vivo* Imaging Using Rare-Earth Nanocrystals with Near-Infrared to Near-Infrared (NIR-to-NIR) Upconversion Luminescence and Magnetic Resonance Properties. *Biomaterials* **2010**, *31*, 3287–3295.
17. Chen, F.; Bu, W. B.; Zhang, S. J.; Liu, X. H.; Liu, J. N.; Xing, H. Y.; Xiao, Q. F.; Zhou, L. P.; Peng, W. J.; Wang, L. Z.; *et al.* Positive and Negative Lattice Shielding Effects Co-existing in Gd (III) Ion Doped Bifunctional Upconversion Nanoprobes. *Adv. Funct. Mater.* **2011**, *21*, 4285–4294.
18. Johnson, N. J. J.; Oalden, W.; Stanisz, G. J.; Prosser, R. S.; van Veggel, F. C. J. M. Size-Tunable, Ultrasmall $NaGdF_4$ Nanoparticles: Insights into Their T1MRI Contrast Enhancement. *Chem. Mater.* **2011**, *23*, 3714–3722.
19. De Jong, W. H.; Hagens, W. I.; Krystek, P.; Burger, M. C.; Sips, A.; Geertsma, R. E. Particle Size-Dependent Organ Distribution of Gold Nanoparticles after Intravenous Administration. *Biomaterials* **2008**, *29*, 1912–1919.
20. Pan, Y.; Neuss, S.; Leifert, A.; Fischler, M.; Wen, F.; Simon, U.; Schmid, G.; Brandau, W.; Jahnen-Dechent, W. Size-Dependent Cytotoxicity of Gold Nanoparticles. *Small* **2007**, *3*, 1941–1949.
21. Semmler-Behnke, M.; Kreyling, W. G.; Lipka, J.; Fertsch, S.; Wenk, A.; Takenaka, S.; Schmid, G.; Brandau, W. Biodistribution of 1.4- and 18-nm Gold Particles in Rats. *Small* **2008**, *4*, 2108–2111.
22. Il Park, Y.; Kim, J. H.; Lee, K. T.; Jeon, K. S.; Bin Na, H.; Yu, J. H.; Kim, H. M.; Lee, N.; Choi, S. H.; Baik, S. I.; *et al.* Nonblinking and Nonbleaching Upconverting Nanoparticles as an Optical Imaging Nanoprobe and T1 Magnetic Resonance Imaging Contrast Agent. *Adv. Mater.* **2009**, *21*, 4467–4471.
23. Boyer, J. C.; Manseau, M. P.; Murray, J. I.; van Veggel, F. C. J. M. Surface Modification of Upconverting $NaYF_4$ Nanoparticles with PEG-Phosphate Ligands for NIR (800 nm) Biolabeling within the Biological Window. *Langmuir* **2010**, *26*, 1157–1164.
24. Caravan, P.; Farrar, C. T.; Frullano, L.; Uppal, R. Influence of Molecular Parameters and Increasing Magnetic Field Strength on Relaxivity of Gadolinium- and Manganese-based T1 Contrast Agents. *Contrast Media Mol. Imaging* **2009**, *4*, 89–100.

25. Caravan, P. Protein-Targeted Gadolinium-Based Magnetic Resonance Imaging (MRI) Contrast Agents: Design and Mechanism of Action. *Acc. Chem. Res.* **2009**, *42*, 851–862.
26. Majonis, D.; Herrera, I.; Ornatsky, O.; Schulze, M.; Lou, X. D.; Soleimani, M.; Nitz, M.; Winnik, M. A. Synthesis of a Functional Metal-Chelating Polymer and Steps toward Quantitative Mass Cytometry Bioassays. *Anal. Chem.* **2010**, *82*, 8961–8969.
27. Saleh, M. N.; Raisch, K. P.; Stackhouse, M. A.; Grizzle, W. E.; Bonner, J. A.; Mayo, M. S.; Kim, H. G.; Meredith, R. F.; Wheeler, R. H.; Buchsbaum, D. J. Combined Modality Therapy of A431 Human Epidermoid Cancer Using Anti-EGFr Antibody C225 and Radiation. *Cancer Biother. Radiopharm.* **1999**, *14*, 451–463.
28. Cai, W. B.; Chen, K.; He, L. N.; Cao, Q. Z.; Koong, A.; Chen, X. Y. Quantitative PET of EGFR Expression in Xenograft-Bearing Mice Using ^{64}Cu-labeled Cetuximab, a Chimeric anti-EGFR Monoclonal Antibody. *Eur. J. Med. Mol. Imaging* **2007**, *34*, 850–858.
29. Teicher, B. A. Tumor Models for Efficacy Determination. *Mol. Cancer Ther.* **2006**, *5*, 2435–2443.